Atmos. Chem. Phys. Discuss., 15, 22141–22182, 2015
www.atmos-chem-phys-discuss.net/15/22141/2015/
doi:10.5194/acpd-15-22141-2015

Atmospheric Chemistry and Physics Discussions
Open Access

Polar Stratospheric Cloud evolution and chlorine activation measured by CALIPSO and MLS, and modelled by ATLAS

H. Nakajima[1,2,a], I. Wohltmann[2], T. Wegner[3], M. Takeda[4], M. C. Pitts[3], L. R. Poole[5], R. Lehmann[2], M. L. Santee[6], and M. Rex[2]

[1]National Institute for Environmental Studies, Tsukuba, 305-8506, Japan
[2]Alfred Wegener Institute for Polar and Marine Research, Potsdam, 14473, Germany
[3]NASA Langley Research Center, Hampton, Virginia, 23681, USA
[4]Graduate School of Tohoku University, Sendai, 980-8579, Japan
[5]Science Systems and Applications, Incorporated, Hampton, Virginia 23666, USA
[6]Jet Propulsion Laboratory, California Institute of Technology, Pasadena, California 91109, USA
[a]now at: Council for Science, Technology and Innovation, Cabinet Office, Government of Japan, Tokyo, 100-8914, Japan

Received: 23 June 2015 – Accepted: 7 July 2015 – Published: 18 August 2015

Correspondence to: H. Nakajima (nakajima@nies.go.jp)

Published by Copernicus Publications on behalf of the European Geosciences Union.

Abstract

We examined observations of polar stratospheric clouds (PSCs) by CALIPSO and of HCl, ClO and HNO_3 by MLS along air mass trajectories to investigate the dependence of the inferred PSC composition on the temperature history of the air parcels, and the dependence of the level of chlorine activation on PSC composition. Several case studies based on individual trajectories from the Arctic winter 2009/10 were conducted, with the trajectories chosen such that the first processing of the air mass by PSCs in this winter occurred on the trajectory. Transitions of PSC composition classes were observed to be highly dependent on the temperature history. In cases of a gradual temperature decrease, nitric acid trihydrate (NAT) and super-cooled ternary solution (STS) mixture clouds were observed. In cases of rapid temperature decrease, STS clouds were first observed, followed by NAT/STS mixture clouds. When temperatures dropped below the frost point, ice clouds formed, and then transformed into NAT/STS mixture clouds when temperature increased above the frost point. The threshold temperature for rapid chlorine activation on PSCs is approximately 4 K below the NAT existence temperature, T_{NAT}. Furthermore, simulations of the ATLAS chemistry and transport box model along the trajectories were used to corroborate the measurements and show good agreement with the observations. Rapid chlorine activation was observed when an airmass encountered PSCs. The observed and modelled dependence of the rate of chlorine activation on the PSC composition class was small. Usually, chlorine activation was limited by the amount of available $ClONO_2$. Where $ClONO_2$ was not the limiting factor, a large dependence on temperature was evident.

1 Introduction

Soon after the discovery of the Antarctic "ozone hole" (Farman et al., 1985), it was established that heterogeneous reactions on polar stratospheric clouds (PSCs) play an important role in ozone destruction (Solomon et al., 1986). They are the first step

ACPD
15, 22141–22182, 2015

in the conversion of chlorine reservoir species ($ClONO_2$ and HCl) to highly reactive radical species (Cl, ClO) which drive catalytic cycles that destroy ozone (e.g., Molina and Molina, 1987).

PSC particles may be solid, consisting of ice (cf. the historical overview by Peter and Grooß, 2012) or nitric acid trihydrate (NAT) (Crutzen and Arnold, 1986; Voigt et al., 2000). Alternatively, they may also be liquid H_2O-H_2SO_4-HNO_3 droplets (super-cooled ternary solution = STS) (Carslaw et al., 1994). Liquid and solid particles can coexist over a wide range of conditions (Koop et al., 1997; Pitts et al., 2009).

The mechanisms by which NAT particles are formed have provoked some controversy (for a review, see Peter and Grooß, 2012). Laboratory measurements have shown that homogeneous nucleation of NAT in H_2O-H_2SO_4-HNO_3 solutions is kinetically limited, and thus cannot be expected immediately after the existence temperature of NAT ($T_{NAT} \approx 195$ K in the lower stratosphere) is reached (Koop et al., 1995). Another proposed NAT formation mechanism is heterogeneous nucleation on ice particles (Koop et al., 1995), which requires temperatures below the ice frost point ($T_{ice} \approx 188$ K in the lower stratosphere). However, NAT PSCs have been observed by both in-situ aircraft and satellite measurements in air masses that had not been exposed to temperatures below T_{ice} (e.g., Pagan et al., 2004; Larsen et al., 2004; Voigt et al., 2005; Pitts et al., 2011). Therefore, heterogeneous nucleation of NAT on meteoritic dust has been considered as an alternative "fast track" to NAT formation at temperatures above the frost point (Voigt et al., 2005; Hoyle et al., 2013).

The uptake of chemical species, e.g. HCl, by PSC particles and the subsequent heterogeneous reaction rates depend on PSC particle composition and surface area density (and strongly on temperature).

Although chlorine activation on PSCs is an essential step towards ozone depletion, under certain conditions the ozone loss may be rather insensitive to the rate constants of those heterogeneous reactions and thus to the composition of PSCs present (e.g., Drdla and Schoeberl, 2003; Wohltmann et al., 2013). For instance, this sensitivity is expected to be small if the PSCs exist long enough so that one reaction partner of

ACPD
15, 22141–22182, 2015

a heterogeneous reaction becomes almost completely depleted. It is also small if one of the reaction partners has already been depleted and its re-generation by gas-phase chemistry is slower than the heterogeneous reactions.

According to the above-mentioned findings, the following questions are relevant for understanding ozone depletion:

1. Which PSC compositions form under which conditions?

2. How sensitively do chlorine activation and, consequently, ozone depletion depend on PSC composition?

In order to investigate Question 1, we used PSC observations by the CALIOP (Cloud–Aerosol Lidar with Orthogonal Polarization) instrument on the CALIPSO (Cloud–Aerosol Lidar and Infrared Pathfinder Satellite Observations) satellite in the Arctic winter 2009/10 and temperature data from ECMWF (European Centre for Medium-Range Weather Forecasts) analyses on backward trajectories initiated at the locations of the PSC observations. All three PSC compositions mentioned above (STS, NAT, ice) were observed. These analyses show that the PSC particle composition depends not only on the temperature at the time of the observation, but also on the temperature history of the air parcel. This conclusion is in agreement with the findings of Lambert et al. (2012), who used a similar approach with CALIOP PSC composition and Aura Microwave Limb Sounder (MLS) HNO_3 data to analyse PSC and HNO_3 evolution.

In order to study Question 2, we investigated the temporal evolution of HCl in the vicinity of observed PSCs. For this, we calculated backward and forward trajectories from the positions of the CALIOP PSC observations and considered Aura MLS HCl measurements within a certain distance ("Match radius") from those trajectories. The signature of chlorine activation seen in the HCl data was compared to simulations from the Lagrangian chemistry-transport model ATLAS (Wohltmann et al., 2010). Additional runs of this model were carried out to estimate the sensitivity of chemical ozone depletion to different PSC compositions.

ACPD
15, 22141–22182, 2015

We concentrated on the time period of the first occurrence of PSCs during the winter (mid-December 2009–beginning of January 2010). This choice allowed us to rule out the prior existence of PSCs and associated repartitioning of chlorine-containing species by heterogeneous reactions. This winter was one of the coldest winters in the Arctic during the CALIPSO operation period when ice PSC was observed by the CALIOP measurements.

2 Data

2.1 CALIPSO/CALIOP PSC data

CALIPSO, a component of the A-train satellite constellation (Winker et al., 2007, 2009), was launched in April 2006 into a 98.2° inclination orbit that provides extensive daily measurement coverage over the polar regions of both hemispheres up to 82° in latitude. CALIOP, the primary instrument on CALIPSO, measures backscatter at wavelengths of 1064 and 532 nm, with the 532 nm signal separated into orthogonal polarization components parallel and perpendicular to the polarization plane of the outgoing laser beam.

Pitts et al. (2007, 2009, 2011) developed a procedure for detecting PSCs using the CALIOP 532 nm scattering ratio (R_{532}, the ratio of total to molecular backscatter) and the 532 nm perpendicular backscatter coefficient. They further developed an algorithm to classify PSCs by composition based on the measured CALIOP aerosol depolarization ratio (δ_{aerosol}, the ratio of perpendicular to parallel components of aerosol backscatter) and inverse scattering ratio ($1/R_{532}$). Pitts et al. (2009) defined four composition classes of PSCs, i.e., STS, ice, Mix 1, and Mix 2. Mix 1 and Mix 2 denote mixtures of liquid droplets with NAT particles in lower or higher number densities/volumes, respectively. Pitts et al. (2011) added two additional sub-classes of PSCs, i.e., Mix 2 enhanced, and wave ice PSCs.

ACPD
15, 22141–22182, 2015

In this study, we used three categories of PSCs from CALIOP data: STS, Mix (which includes Mix 1, Mix 2, and Mix 2 enhanced), and ice (which includes ice and wave ice) PSCs.

In order to assign PSC composition along the trajectories, we selected the composition of the CALIOP measurement location that was closest to each trajectory point. For each trajectory point, the horizontally closest CALIOP measurement profile was first determined and then the PSC classification closest in potential temperature to the trajectory point was taken from this measurement profile. An analogous method was used to produce the maps in Fig. 2.

Due to the sampling pattern of CALIOP, there is some intrinsic and unavoidable uncertainty in the PSC characterizations at any given location, which is typically some distance away from the point being measured by CALIOP. The approach we have used relies on the assumption that PSCs are sufficiently homogeneous on a spatial scale that corresponds to the average distance to the next measurement, which is about 100–200 km.

2.2 MLS data

This study also uses data from the Microwave Limb Sounder (MLS) instrument on the Aura satellite (Waters et al., 2006). The Earth Observing System (EOS) Aura satellite was launched on 15 July 2004 and has been in operation since August 2004 making measurements between 82° N and 82° S. MLS measures millimeter- and submillimeter-wave thermal emission from the limb of Earth's atmosphere. We use MLS version 3.3 HCl, ClO, HNO_3, and O_3 data (Livesey et al., 2006, 2013). Vertical resolution of MLS data is ~ 3 km in the lower stratosphere at 100–10 hPa. A discussion of the quality of MLS measurements can be found in Livesey et al. (2013). Error bars in the figures that follow indicate the 1σ precision of the measurements.

ACPD
15, 22141–22182, 2015

3 Analysis method

3.1 PSC evolution in the northern winter 2009/10

In the Arctic winter 2009/10, PSCs started to appear in mid-December 2009 at around 23 km when the minimum temperature dropped below the nitric acid trihydrate saturation temperature T_{NAT} (Pitts et al., 2011). Figure 1 shows the temporal variation of the minimum temperature (T_{MIN}) between 50 and 90° N at the 30 hPa pressure level. The thick black line is the mean over the winters 1978/79 to 2013/14, while the thin black lines are minimum and maximum temperatures. The thick red line shows the variation of the daily minimum temperature in the 2009/10 Arctic winter. The two green lines show the NAT and ice PSC threshold temperatures (T_{NAT} and T_{ice}, respectively) calculated by assuming 6 ppbv of HNO_3 and 4.5 ppmv of H_2O. T_{MIN} dropped below T_{NAT} at the middle of December and below T_{ice} at the end of December 2009 and again in mid-January. A sudden stratospheric warming terminated the period with temperatures below T_{NAT} at the end of January 2010 (Dörnbrack et al., 2012).

The PSC observations of CALIOP are consistent with the temperature history in this winter. Figure 2a shows an example of the PSC field on the 550 K potential temperature surface for 21 December 2009 with CALIOP observation points, when substantial PSC coverage was first observed by CALIOP at this altitude (~ 23 km) in this Arctic winter. Note that the CALIOP PSC products are only produced for nighttime orbit segments due to higher background lighting conditions during daytime. On 21 December 2009, the day/night transition occurs near 72° N. Also note that the area north of 82° N is shadowed by grey color, because there is no CALIPSO orbital coverage there. Similarly, Fig. 2b shows an example of the PSC field at 550 K for 1 January 2010, when the maximum extent of PSCs was observed at this altitude. PSC fields were created in this way for each day during the 2009/10 Arctic winter.

ACPD
15, 22141–22182, 2015

3.2 Selection of trajectories for the case studies

As mentioned in Sect. 1, backward and forward trajectories from the positions of CALIOP PSC observations were calculated, in order to investigate the chemical effects of these PSCs by analysing chemical model runs and trace gas observations along these trajectories. In order to exclude any chemical effect of earlier PSCs in the analysed air masses, we concentrate on the time period of early winter (between 19 December 2009 and 3 January 2010).

As a first step, several cases of CALIOP observations of PSCs of a clearly defined composition class were selected. The selected cases encompass a range of different conditions with respect to temperature and PSC classification. Two examples are presented in Figs. 3 and 4. In each case, a location in the center of such a PSC was selected. It was marked by a cross and a label in Fig. 3a ("n1": mix 1 PSC), and Fig. 4a ("e4": mix 2 enhanced PSC). In order to show the temporal evolution of temperature and HCl in the analysed airmass, 5 day backward and 5 day forward trajectories, starting at the marked position, were calculated. The corresponding trajectory model is taken from the ATLAS chemistry and transport box model (Wohltmann et al., 2010). Model runs are driven by meteorological data from the ECMWF ERA Interim reanalysis (Dee et al., 2011), with time resolution of 6 h and horizontal resolution of 2 times 2°. The vertical coordinate is potential temperature and vertical motion is driven by total diabatic heating rates from ERA Interim.

Figures 3b and 4b show MLS measurements of HCl along the path of the trajectories as a function of time (green dots with error bars). All HCl measurements that were closer than 200 km to the position of the trajectory at a given point in time are plotted. PSC occurrence is color coded in the background. Green shaded areas correspond to STS clouds, red shaded areas to NAT/STS mixture clouds, and blue shaded areas correspond to ice clouds. Grey areas correspond to sections of the trajectory north of 82° N, where no measurements from CALIOP or MLS are available. Nevertheless, we can find some matched MLS points within the grey area in Fig. 3b. This is because MLS

ACPD
15, 22141–22182, 2015

observations were selected within a match radius of 200 km. Figures 3b and 4b show that HCl values were around 2 ppbv on the backward trajectories and that either no PSCs were measured by CALIOP or no measurements from CALIOP were available on the backward trajectory. HCl started to decrease near $t = 0$, a time at which PSCs were present according to our choice of the trajectory starting points. Figures 3c and 4c show the temperature along the trajectories, with the PSC occurrence as in Figs. 3b and 4b. The thin black lines correspond to T_{NAT} and $T_{NAT} - 3$ K, the thin blue line corresponds to T_{ice}. The threshold temperature for the formation of NAT clouds (T_{NAT}) is based on the equations of Hanson and Mauersberger (1988). For the forward part of the trajectory, HNO_3 and H_2O from the box model runs (cf. Sect. 4) were used for the calculation of T_{NAT}. For the backward part of the trajectory, HNO_3 and H_2O values were fixed at the starting values of the box model run. The threshold temperature for the formation of ice (T_{ice}) was calculated in the same manner from the equations of Marti and Mauersberger (1993). In the cases shown in Figs. 3 and 4, the temperature does not drop below $T_{NAT} - 3$ K on the backward trajectory (before the occurrence of selected PSC). It can be seen that when temperature decreased, PSCs started to form along the path of the forward trajectory.

In order to analyse the temporal evolution of chemical species after the encounter of PSCs, ATLAS box model runs, which will be explained in the following Section in detail, will be performed on several trajectory cases. It is desirable to start these model runs from initial concentrations that have not been influenced by any earlier PSC occurrence in the airmass of interest. However, if these model runs started at the locations selected in the center of a PSC (as those marked in Figs. 3a and 4a), then a part of the backward trajectory would lie within the selected PSC. Consequently, some chlorine activation might occur already before the beginning of the forward trajectory. In order to avoid this effect, the forward trajectories for the runs of the ATLAS box model are started before the encounter of the selected PSC. For this, a new starting point (corresponding to a new starting time $t = 0$) of the trajectory calculations was selected on the original backward trajectory such that it fulfills the following conditions: (1) there is no

ACPD
15, 22141–22182, 2015

PSC in the CALIOP data near the backward trajectory before the new starting time. (2) The temperature at and before the new starting time does not drop below $T_{NAT} - 3$ K. The assumption behind this is that a supersaturation of about 10 (3 K supercooling) is needed for the formation of NAT clouds and that STS clouds only take up measureable quantities of HNO_3 below $T_{NAT} - 3$ K. (3) The matched MLS HCl values at and before the new starting time were above ~ 2 ppbv, which proves that the airmass has not been processed by PSCs before the new $t = 0$. In such a way, we selected ~ 30 trajectory cases in early winter between 19 December 2009 and 3 January 2010 for several PSC classes. Then we selected 11 new trajectory starting points (summarised in Table 1) for case studies. Starting from these points, new 5-days forward and 5-days backward trajectories were calculated. ATLAS box model was run on these 5-days forward trajectories, which passed through the center part of the selected PSCs.

4 ATLAS model

4.1 Model description

The box model runs, simulating the temporal evolution of chemical species along the trajectories described in Sect. 3.2, use the chemistry box model of the ATLAS (Wohltmann et al., 2010). Updates to the chemistry model and PSC model are described in Wohltmann et al. (2013). The model includes a gas phase stratospheric chemistry module and heterogeneous chemistry on PSCs. It comprises 47 active species and more than 180 reactions. Absorption cross sections and rate coefficients are taken from recent JPL recommendations (Sander et al., 2011). The chemical model runs are driven by meteorological data from the ECMWF ERA Interim reanalysis.

The treatment of conditions where both NAT and STS PSCs are allowed to form in the model has changed compared to Wohltmann et al. (2013) to allow for more realistic behavior. In Wohltmann et al. (2013), only liquid clouds could form between T_{NAT} and the temperature corresponding to the assumed supersaturation for HNO_3 over NAT.

ACPD
15, 22141–22182, 2015

At temperatures below that of the assumed supersaturation, NAT clouds would form first, usually consuming all available HNO_3 and impeding the formation of ternary liquid clouds (by chance, the temperature where binary liquid aerosols begin to take up HNO_3 in measurable quantities is about the same as the temperature where NAT clouds begin to form in the model). Since NAT/STS mixtures are commonly observed (e.g. Pitts et al., 2011), we implemented a simple algorithm that allows for mixed clouds: if the given supersaturation of HNO_3 over NAT is exceeded, only a predefined fraction of the amount of HNO_3 that has to be removed from the gas phase to reach the supersaturation again is allowed to go into NAT clouds. The remaining fraction is available for the formation of STS clouds. The fraction is set to 0.2 for our model runs.

4.2 Sensitivity runs

Three sensitivity runs with different assumptions on PSCs are performed for each trajectory. In the "STS + NAT" run, PSC information from CALIPSO is ignored and the box model forms PSCs according to temperature and available condensable HNO_3 and H_2O, in the same way as described in Sect. 4.1. In this run, the NAT particle number density is set to 0.1 cm^{-3}, the ice particle number density is set to 0.01 cm^{-3}, and the STS droplet number density is set to 10 cm^{-3}. A supersaturation of HNO_3 over NAT of 10 (corresponding to about 3 K supercooling) is required for NAT particle formation. A detailed discussion of the rationale behind these choices can be found in Wohltmann et al. (2013). For ice particles formation, a supersaturation of 0.35 is assumed based on MLS satellite measurements of H_2O and ECMWF temperatures. Reaction rates for NAT particles are based on scheme 1 in Carslaw et al. (1997) and reaction rates for liquid particles are based on Hanson and Ravishankara (1994).

The "STS" run is identical to the "STS + NAT" run, except that no NAT clouds are allowed to form.

The "CALIPSO constrained" run uses the information from the CALIPSO satellite to constrain the formation of PSC within the model. Five different cases are considered:

ACPD
15, 22141–22182, 2015

1. If CALIOP measures no PSCs, no clouds are formed in the box model runs.
2. If CALIOP detects only STS, then STS is allowed to form according to temperature and species mixing ratios in the box model, as explained above. Note that in the "STS + NAT" and "STS" runs, STS may form outside of the area where CALIOP detects STS clouds, if the temperature conditions are appropriate. However, in the "CALIPSO constrained" run, the model will not form STS outside of the area where CALIOP detects STS. In addition, if CALIOP detects STS in a region where ECMWF temperatures are too warm for STS existence, the model will only produce binary liquid aerosol.
3. If CALIOP detects mixed clouds, both STS and NAT clouds are simulated in the box model. STS clouds are simulated in the same way as above. NAT clouds are formed with a predefined number density of 10^{-3} cm^{-3} and a predefined radius of 2 µm.
4. If CALIOP detects ice clouds, ice clouds are formed with a predefined number density of 1 cm^{-3} and a predefined radius of 5 µm.
5. There are no CALIOP measurements north of 82° N. In this region, the "CALIPSO constrained" run uses the same setting as the "STS + NAT" run.

The NAT and ice cloud number densities used here were derived by comparing the 2-D histograms of CALIOP PSC observations (Fig. 4 in Pitts et al., 2009) and theoretical calculation of NAT and ice PSC growth (Figs. 5 and 6 in Pitts et al., 2009). Note that while these numbers are plausible under atmospheric conditions, particles in the real atmosphere may exist over a wide range of sizes and number densities (e.g., Wegner et al., 2012).

4.3 Chemical initialization

The model chemical initialization is performed in three steps. First, all of the species are initialized from the mixing ratio fields of an existing global model run of ATLAS for

ACPD
15, 22141–22182, 2015

the winter 2009/10 (the reference run in Wohltmann et al., 2013). For this, a short back trajectory is calculated from the starting position of each trajectory back to the time of the last model output of the global model run preceding the start date of the trajectory. The chemical model is then run forward on this short trajectory with the initialization taken from the nearest air parcel of the global model output.

In the second step, mixing ratio values for HCl, O_3 and H_2O are replaced by measurements from MLS. MLS gas-phase HNO_3 observations are not used, in order to avoid problems when some of the total available HNO_3 is in the condensed phase (the model needs total HNO_3 and MLS measures gas phase HNO_3). The MLS values for HCl, O_3 and H_2O are obtained by calculating a 5 day back trajectory from the starting point of each trajectory and calculating an average over all MLS measurements close to the trajectory (with a match radius of 200 km). In order to keep Cl_y (the sum of all inorganic species containing chlorine) constant at the value specified by the global ATLAS runs, the difference between the MLS HCl value and the HCl value of the global model run is added to (or subtracted from, depending on sign) the mixing ratio of $ClONO_2$. Note that no chlorine activation has yet taken place at the time when the model is initialized, and this correction does not produce negative $ClONO_2$ values for any of the trajectories.

In some cases (trajectories #05, #08, and #10), modelled $ClONO_2$ is fully depleted before HCl reaches the level indicated by the MLS measurements. In these cases, a third step is applied to ensure that HCl and $ClONO_2$ are adjusted such that the amount of HCl loss in the model matches the loss of HCl in the MLS data. In all of these cases, there is a significant difference between the observed HCl mixing ratios before and after the PSC occurrence. The magnitude of this observed drop in HCl is used as the initialization for $ClONO_2$, such that $ClONO_2$ is nearly depleted at the end of the box model run. In order to keep Cl_y constant again, the difference between the new $ClONO_2$ value (taken from the decrease in observed HCl) and the old $ClONO_2$ value (after the first correction in the second step caused by MLS HCl) is added to (or subtracted from) $ClO_x = ClO + 2Cl_2O_2$ in a way that preserves the partitioning between ClO and Cl_2O_2.

ACPD
15, 22141–22182, 2015

5 Results

5.1 Dependence of PSC classification on temperature history

In this section, we show the temporal change in PSC classification along nine selected trajectories with different temperature histories.

Figure 5a–c shows cases in which the airmass cooled gradually over a period of days to below $T_{NAT} - 3$ K. NAT/STS mixture PSCs started to appear when the airmass temperature decreased below approximately $T_{NAT} - 4$ K in all cases shown. No ice PSCs and only a negligible amount of STS PSCs were observed during the course of the trajectory. When temperatures warmed above T_{NAT}, the mixed PSCs mostly disappeared. Since there was no region within the polar vortex with temperatures below the frost point before these PSC events, the NAT/STS mixture PSC observed here was assumed to be formed without any prior exposure to ice PSCs.

Figure 6a–c shows cases in which the airmass temperature decreased rather rapidly due to adiabatic cooling by orographic lift as it passed over Greenland. In these cases, STS formed first as the temperature decreased below approximately $T_{NAT} - 4$ K, followed by a transition to NAT/STS mixture PSCs as the temperature warmed to near T_{NAT}. When the temperature rose above T_{NAT}, the PSCs disappeared.

Figure 7a–c shows cases where the airmass temperature decreased rapidly to T_{ice} due to adiabatic cooling by orographic lift as it passed over Greenland. In these cases, STS formed first as the temperature decreased below approximately $T_{NAT} - 4$ K, followed by the formation of ice as the temperature decreased to T_{ice}. As the temperature warms above T_{ice}, the ice PSC is transformed into a NAT/STS mixture PSC, as suggested by an old theory of NAT PSC formation. With the exception of the #10 case, the CALIOP ice PSC observations coincide quite well with the trajectory segments with airmass temperatures below T_{ice}. This proves the accuracy of ECMWF ERA Interim reanalysis temperature data to some extent even in a mesoscale scenario such as mountain-induced adiabatic cooling event. However, as will be discussed later, our model runs suggest that the uncertainty in ECMWF temperature is about 1 K.

ACPD
15, 22141–22182, 2015

5.2 Comparison of MLS measurements with the ATLAS model

In this section, we show the temporal changes of several parameters modelled by ATLAS and compare these with Aura/MLS measurements.

Figure 8a–i shows the trajectory case #03 that started at 07:58:21 UT on 23 December 2009. It is not known if PSCs existed between 8 and 49 h after the starting time of the forward trajectory because the trajectory went into the polar region above 82° N latitude where there are no CALIOP measurements. At hour 49, the airmass encountered STS and then NAT/STS mixture PSCs as the temperature cooled below approximately $T_{NAT} - 4$ K as shown in Fig. 8a. The surface area densities of the PSCs calculated by ATLAS for the three different sensitivity runs, i.e. the STS + NAT run, STS run, and "CALIPSO constrained run" are shown in Fig. 8b. ATLAS indicated a small increase in surface area density between days 1 and 2 when the temperature decreased approximately 4 K below T_{NAT}, where CALIOP was not able to measure in that period due to the sampling limitation stated above. Similarly, the calculated heterogeneous reaction rate of $ClONO_2$ + HCl on the PSC particles is shown in Fig. 8c. Note that the reaction rate decreased more rapidly than the surface area of the PSCs. This is due to the total loss of $ClONO_2$ as will be discussed later in detail. Figure 8d shows the calculated and measured amount of HCl by ATLAS and by Aura/MLS, respectively. MLS observations were matched to the trajectory with a match radius of 200 km, as was explained in Sect. 3.2. When the temperature decreased to about $T_{NAT} - 3$ K, the calculated HCl started to decrease in all three model runs. Similarly, $ClONO_2$ started to decrease and was fully depleted between days 2 and 3 as is shown in Fig. 8e. After this point, HCl could not decrease anymore because the reaction partner ($ClONO_2$) was already fully depleted. The measured and calculated HCl values agree quite well within the error bars of MLS measurements as expected. The depleted chlorine was converted into ClOx as is shown in Fig. 8f. Because little sunlight was present along the trajectory, only a small amount of ClOx exists in the form of ClO as is shown in Fig. 8g after day 4. Figure 8h shows the calculated and measured amount of HNO_3

ACPD
15, 22141–22182, 2015

by ATLAS and by Aura/MLS, respectively. In the three different ATLAS model runs, different HNO_3 values were calculated. However, MLS HNO_3 values were much smaller than the modelled values in all three model runs after day 3. Since the denitrification module of the global ATLAS model is designed to work correctly only on larger spatial and time scales, it cannot reproduce the denitrification for a single trajectory correctly. Modelling HNO_3 correctly by ATLAS along individual trajectories is beyond the scope of this paper. Figure 8i shows the calculated and measured amount of O_3 by ATLAS and by Aura/MLS, respectively. Since there was not sufficient ClO available for catalytic ozone destruction due to the lack of solar illumination, both calculated and measured O_3 did not indicate any ozone depletion in this case.

Figure 9a–i shows the trajectory case #05 that started at 17:53:38 UT on 30 December 2009. The trajectory encountered a region of CALIOP STS measurements after 10 h as the temperature decreased below approximately $T_{NAT} - 5$ K. Between days 1 and 5, NAT/STS mixture PSCs were observed along the trajectory, as well as a very short period of ice PSCs between days 1 and 2 when the temperature cooled to T_{ice}. Calculated PSC surface area density increased rapidly when the airmass temperature decreased below around $T_{NAT} - 3$ K between days 0 and 2 as is shown in Fig. 9b. However, both HCl and $ClONO_2$ stopped decreasing just a few hours after the airmass encountered the STS PSCs, because the $ClONO_2$ was fully depleted within this time as is shown in Fig. 9d and e. The measured and calculated HCl values agree quite well. The depleted reservoir chlorine was first converted into Cl_2, then after exposure to sunlight (indicated by orange dots on the upper part of Fig. 9d–i), Cl_2 was photolyzed to form ClO_x (Fig. 9f and g). The measured and calculated ClO values also agree quite well. The temporal evolution of HNO_3 is shown in Fig. 9h. The measured HNO_3 between days 2 and 5 is slightly depleted, suggesting the possibility of mild denitrification. A small amount of ozone depletion was modelled by ATLAS in this case when sufficient ClO was available as is shown in Fig. 9i.

Figure 10a–i shows the trajectory case #08 that started at 16:59:14 UT on 31 December 2009. After 3 h, the airmass encountered STS PSCs as the temperature decreased

ACPD
15, 22141–22182, 2015

below approximately $T_{NAT}-5$ K. As the temperature further decreased to reach T_{ice} after 20 h, ice PSCs were observed by CALIOP as is shown in Fig. 10a. When the temperature increased above T_{ice} after 23 h, NAT/STS mixture PSCs were observed. This case is quite similar to the previous case. Calculated PSC surface area density rapidly increased when the airmass cooled to around T_{ice} between days 0 and 2 as shown in Fig. 10b. However, both HCl and $ClONO_2$ stopped decreasing just a few hours after the airmass encountered STS PSCs, because $ClONO_2$ was fully depleted within this time as shown in Fig. 10d and e. Also in this case, the measured and calculated HCl values agree quite well. The depleted reservoir chlorine was first converted into Cl_2, then with exposure to sunlight (indicated by orange dots on the upper part of Fig. 10d–i), Cl_2 was photolyzed to form ClO as shown in Fig. 10g. The MLS HNO_3 values were slightly depleted between days 1 and 3, suggesting the possibility of a small degree of denitrification. In this case, slight ozone destruction was modelled by ATLAS when there was sufficient ClO available, as is shown in Fig. 10i. However, the uncertainty in the measured ozone is too large to deduce a quantitative ozone loss amount.

5.3 Temperature sensitivity study for ATLAS model runs

Figure 11a–i shows the trajectory case #02 that started at 08:09:30 UT on 21 December 2009. After 55 h, the airmass encountered STS PSCs as the temperature decreased below $T_{NAT}-4$ K for a while. Shortly afterwards, a mixed type PSC was observed by CALIOP. When temperature increased to around T_{NAT} at day 4, STS PSC was observed again before the airmass exited the PSC area. In this case, the time period when the temperature was below $T_{NAT}-4$ K was relatively short as is shown in Fig. 11a. As a result, the higher values of PSC surface area calculated by ATLAS were limited to a short time period at around day 2 as is shown in Fig. 11b. As a result, the decrease of both HCl and $ClONO_2$ modelled by ATLAS was small, and $ClONO_2$ was not totally depleted even after passage through the PSCs. In addition, the modelled HCl and $ClONO_2$ are very sensitive to different PSC scenarios that are assumed in this case. The STS + NAT model run produces the largest decrease in the chlorine reser-

ACPD
15, 22141–22182, 2015

voirs, while the CALIPSO-constrained model run produces the smallest decrease in the chlorine reservoirs. Moreover, all three model runs underestimate the loss of HCl compared with observations as is shown in Fig. 11d.

In order to study the sensitivity of the ATLAS model runs to the ECMWF ERA Interim reanalysis temperatures, we made additional ATLAS model runs by introducing a ±1 K temperature bias. Figure 12a–i shows the same trajectory as Fig. 11a–i with red and blue lines added to show the sensitivity runs with the temperature changed by ±1 K, respectively. The reference run (black line) is the STS + NAT run. As is shown in Fig. 12b and c, a temperature change of only 1 K greatly affects the PSC surface area density and heterogeneous reaction rate of $ClONO_2$ + HCl. As a result, the modelled depletion of HCl and $ClONO_2$ are also significantly affected as is shown in Fig. 12d and e. In fact, the minus 1 K model run result agrees fairly well with the MLS HCl observations as shown in Fig. 12d. This result suggests that very accurate temperature data are required to correctly model the heterogeneous reactions on PSCs at temperatures near $T_{NAT} - 4$ K.

Figure 13a–i shows another example; trajectory case #09 which started at 18:35:15 UT on 31 December 2009. After 18 h, the airmass encountered NAT/STS mixture PSCs as the temperature decreased below approximately $T_{NAT} - 3$ K. In this case, the time period when the temperature was below $T_{NAT} - 3$ K was very short (less than 10 h), as is shown in Fig. 13a. Accordingly, the modelled increase of PSC surface area density and heterogeneous chlorine activation were very small as is shown in Fig. 13b and c. Consequently, the model did not produce substantial HCl or $ClONO_2$ depletion around day 1, as shown in Fig. 13d and e. However, MLS HCl measurements do indicate some depletion between days 2 and 4, as shown in Fig. 13d. These results again suggest the uncertainty of ECMWF temperature compared with the actual temperature.

Figure 14a–i shows the results of the temperature sensitivity study for case #09. As shown by Fig. 14b and c, perturbing the ECMWF temperature field by minus 1 K greatly increases the likelihood of PSCs around day 1. Consequently, the modelled

ACPD
15, 22141–22182, 2015

HCl depletion for the minus 1 K case agrees with the MLS measurements quite well as shown in Fig. 14d. This result again illustrates the importance of accurate temperature data especially when the temperature is around $T_{NAT} - 4$ K, which is the approximate threshold temperature of NAT/STS mixture and STS PSC formation.

6 Discussion

In Sect. 5.1, we showed three typical temperature histories for PSC formation, i.e., gradual temperature decrease, rapid temperature decrease, and temperature decrease below T_{ice}. Figure 5a–c shows the formation of NAT/STS mixture PSCs for the case of gradual temperature decrease in airmasses that have never experienced temperatures below T_{ice}. These cases clearly show the existence of an ice-free nucleation mechanism of NAT, as was previously suggested by Drdla et al. (2003), Larsen et al. (2004), Pagan et al. (2004), Voigt et al. (2005), Pitts et al. (2011), and Hoyle et al. (2013). The homogeneous nucleation of NAT in H_2O-H_2SO_4-HNO_3 solutions is kinetically strongly hampered and thus cannot be expected (Koop et al., 1997). One of the possible mechanisms for NAT formation is heterogeneous nucleation on solid particles such as meteoritic dust, as was postulated by Iraci et al. (1995), although Biermann et al. (1996) suggested that heterogeneous nucleation rates on micrometeorites are too low to enable freezing of NAT PSCs. Our results suggest the possibility of heterogeneous nucleation of NAT on solid particles as is already pointed out by Hoyle et al. (2013).

When the airmass temperature cooled rapidly due to adiabatic cooling by passage over mountain ranges, STS PSCs first formed as the temperature decreased below approximately $T_{NAT} - 4$ K as shown in Fig. 6a–c. As the airmass temperature began to increase, a transition to NAT/STS mixture PSCs was observed without the existence of ice, especially for the case #06. Such a case was previously reported in PSC observations by backscatter sondes in the Arctic by Larsen et al. (1997). This result also indicates the possibility of ice-free formation of NAT.

ACPD
15, 22141–22182, 2015

Figure 7a–c shows the cases when the airmass temperature decreased rapidly below T_{ice} due to adiabatic cooling over mountain ranges. As the airmass temperature began to increase, a transition to NAT/STS mixture PSCs was observed in all these cases. NAT/STS mixture PSCs usually disappear when the temperature warms above T_{NAT}. These cases are consistent with the ice-assisted nucleation mechanism of NAT suggested by Carslaw et al. (1995).

In Sect. 5.2, comparisons of MLS HCl, ClO, HNO_3, and O_3 measurements with ATLAS model simulation results were shown for the trajectory cases #03, #05, and #08. Figure 8a–i shows the gradual temperature decrease case #03, Fig. 9a–i show the rapid temperature decrease case #05, and Fig. 10a–i show the temperature decrease below T_{ice} case #08. In all three cases, measured and modelled HCl and ClO agree fairly well, irrespective of the three model scenarios, i.e., "STS + NAT", "STS", and "CALIPSO constrained". The difference in modelled HCl and ClO among the three scenario runs was very small and it is difficult to tell which scenario most closely fits the measurements. In other words, if the airmass cooled below approximately $T_{NAT} - 4$ K for a longer time and consequently there was substantial chlorine activation on PSCs, the PSC classification has little impact on the details of the chlorine activation. The chlorine activation usually occurred very rapidly within a few hours. The amount of HCl loss was shown to be limited by the available $ClONO_2$ amount. After all the $ClONO_2$ has been converted into ClO_x, HCl cannot be further depleted as previously shown in a model study by Müller et al. (1994).

In Sect. 5.3, similar comparison results were shown for the cases #02 and #09, when the airmass temperature was below approximately $T_{NAT} - 4$ K for only a short time period. In these trajectory cases, the depletion of HCl and activation of ClO was underestimated by the model in comparison to the MLS measurements for all three model scenarios, although the "STS + NAT" and "CALIPSO constrained" runs were closer to the measurements than the "STS" run. In these cases, $ClONO_2$ was not totally depleted after passage through the PSCs. In cases where only a small amount of chlorine is activated, the amount of chlorine activation on PSCs is dependent on PSC

ACPD
15, 22141–22182, 2015

classification and/or airmass temperature. In fact, changing the ECMWF ERA Interim temperature field used as input to the ATLAS model by ±1 K has a large impact on the resulting magnitude of chlorine activation as shown in Figs. 12a–i and 14a–i. The large temperature sensitivity around $T_{NAT} - 4$ K can be attributed to the fact that both PSC surface area density and heterogeneous reaction probability (gamma value) increase quite rapidly around this temperature. Therefore, we conclude that quite accurate temperature knowledge is needed to correctly model the chlorine activation amount at around $T_{NAT} - 4$ K.

7 Conclusions

We performed trajectory analyses to study the evolution of PSC composition and chlorine activation from the reservoir species of HCl and $ClONO_2$. We investigated which PSCs form according to measurements of CALIOP as a function of the temperature history along the trajectories. We studied 11 individual trajectories in the early Arctic winter 2009/10. In cases of a gradual temperature decrease below approximately $T_{NAT} - 4$ K, NAT/STS mixture PSCs appeared first. In these cases, ice PSCs were not observed by CALIOP before the formation of the mixed clouds, nor were temperatures below T_{ice} observed. This provides strong additional observational support for the conclusions by Drdla et al. (2003), Larsen et al. (2004), Pagan et al. (2004), Voigt et al. (2005), Pitts et al. (2011), and Hoyle et al. (2013) that NAT clouds can form without the prior formation of ice clouds. Since laboratory experiments suggest that homogenous freezing of NAT is unlikely, a possible mechanism of ice-free formation of NAT could be heterogeneous nucleation on solid particulates such as meteoritic dust (Voigt et al., 2005; Hoyle et al., 2013). When the airmass temperature dropped rapidly due to adiabatic cooling, STS PSCs formed first when the temperature decreased below approximately $T_{NAT} - 4$ K. If the temperature further decreased below T_{ice}, ice PSCs were formed. Then when the airmass temperature started to increase above T_{ice}, NAT/STS mixture PSCs

ACPD
15, 22141–22182, 2015

were formed, as suggested by the formation pathway of NAT clouds from ice clouds (e.g. Carslaw et al., 1995).

We further analysed the chlorine activation process based on MLS observations of HCl and ClO and the ATLAS Chemistry and Transport Model runs. Several sensitivity runs with different temperature histories or different PSC types were conducted. We find that our cases fall in one of two categories.

(1) In most cases chlorine activation occurred sufficiently rapidly, such that the degree of chlorine activation by the first PSC encounter for the respective air mass was limited by the initially available $ClONO_2$, i.e. $ClONO_2$ concentrations fell to very low values. For these cases, ATLAS model results, i.e. the modelled mixing ratios of HCl and ClO_x before and after the chlorine activation by the PSCs, generally agreed well with the MLS observations. The good agreement is expected, since for these cases the degree of chlorine activation only depends on available $ClONO_2$ and is largely insensitive to the rate of the heterogeneous reactions and therefore to the exact PSC composition and temperature. This finding is further illustrated by the fact that all ATLAS sensitivity runs give very similar results for all these cases.

(2) In a few cases, temperatures during the first PSC encounter remained higher (around $T_{NAT} - 4$ K) and the chlorine activation is slower, such that the rates of the heterogeneous reactions integrated over the time of exposure to PSCs limit the degree of chlorine activation, rather than the available amount of $ClONO_2$. In these cases, substantial amounts of $ClONO_2$ can survive the initial PSC encounter and the model is not always able to reproduce the degree of chlorine activation. As expected for these cases, the ATLAS sensitivity runs show that the amount of chlorine activation depends on both, PSC composition and temperature. In particular, the sensitivity to temperature is extremely large in these situations, suggesting that a temperature uncertainty of ±1 K is sufficient to explain most discrepancies between model results and observations. However, based on the data from the winter 2009/10 these situations are fairly rare. $T_{NAT} - 4$ K is an approximate threshold temperature for rapid chlorine activation on PSCs.

ACPD
15, 22141–22182, 2015

Author contributions. H. Nakajima and M. Takeda designed the method of this study. I. Wohltmann developed and ran the ATLAS box model, ran trajectory calculations, and developed the PSC interpolation algorithm. T. Wegner, M. C. Pitts, and L. R. Poole developed and analysed PSC observations from CALIPSO/CALIOP data. M. L. Santee developed and analysed minor species from Aura/MLS data. H. Nakajima, I. Wohltmann, R. Lehmann, and M. Rex discussed on the analysis results. H. Nakajima prepared the manuscript with contributions from all co-authors.

Acknowledgements. We acknowledge European Centre for Medium-Range Weather Forecasts (ECMWF) for providing us with the ERA Interim reanalysis data. One of the authors (H. Nakajima) appreciates the warm hospitality given by all the members of Alfred Wegener Institute for Polar and Marine Research at Potsdam, Germany when he was staying there for half a year as a sabbatical visit. Work at the Jet Propulsion Laboratory, California Institute of Technology, was done under contract with the National Aeronautics and Space Administration.

References

Biermann, U. M., Presper, T., Koop, T., Mößinger, J., Crutzen, P. J., and Peter, T.: The unsuitability of meteoritic and other nuclei for polar stratospheric cloud freezing, Geophys. Res. Lett., 23, 1693–1696, 1996.

Carslaw, K. S., Luo, B. P., Clegg, S. L., Peter, T., Brimblecombe, P., and Crutzen, P. J.: Stratospheric aerosol growth and HNO_3 gas phase depletion from coupled HNO_3 and water uptake by liquid particles, Geophys. Res. Lett., 21, 2479–2482, 1994.

Carslaw, K. S., Peter, T., and Müller, R.: Uncertainties in reactive uptake coefficients for solid stratospheric particles – 2. Effect on ozone depletion, Geophys. Res. Lett., 24, 1747–1750, 1997.

Carslaw, K. S., Wirth, M., Tsias, A., Luo, B. P., Dörnbrack, A., Leutbecher, M., Volkert, H., Renger, W., Bacmeister, J. T., Reimer, E., and Peter, T.: Increased stratospheric ozone depletion due to mountain-induced atmospheric waves, Nature, 391, 675–678, 1998.

Crutzen, P. J. and Arnold, F.: Nitric acid cloud formation in the cold Antarctic stratosphere: a major cause for the springtime "ozone hole", Nature, 324, 651–655, 1986.

Dee, D. P., Uppala, S. M., Simmons, A. J., Berrisford, P., Poli, P., Kobayashi, S., Andrae, U., Balmaseda, M. A., Balsamo, G., Bauer, P., Bechtold, P., Beljaars, A. C. M., van de Berg, L.,

Bidlot, J., Bormann, N., Delsol, C., Dragani, R., Fuentes, M., Geer, A. J., Haimberger, L., Healy, S. B., Hersbach, H., Hólm, E. V., Isaksen, L., Kållberg, P., Köhler, M., Matricardi, M., McNally, A. P., Monge-Sanz, B. M., Morcrette, J.-J., Park, B.-K., Peubey, C., de Rosnay, P., Tavolato, C., Thépaut, J.-N., and Vitart, F.: The ERA-Interim reanalysis: configuration and performance of the data assimilation system, Q. J. Roy. Meteor. Soc., 137, 553–597, 2011.

Dörnbrack, A., Pitts, M. C., Poole, L. R., Orsolini, Y. J., Nishii, K., and Nakamura, H.: The 2009–2010 Arctic stratospheric winter – general evolution, mountain waves and predictability of an operational weather forecast model, Atmos. Chem. Phys., 12, 3659–3675, doi:10.5194/acp-12-3659-2012, 2012.

Drdla, K. and Schoeberl, M. R.: Microphysical modeling of the 1999–2000 Arctic winter, 2, Chlorine activation and ozone depletion. J. Geophys. Res., 108, 8319, doi:10.1029/2001JD001159, 2003.

Drdla, K., Schoeberl, M. R., and Browell, E. V.: Microphysical modeling of the 1999–2000 Arctic winter, 1, Polarstratospheric clouds, denitrification, and dehydration. J. Geophys. Res., 108, 8312, doi:10.1029/2001JD000782, 2003.

Farman, J. C., Gardiner, B. G., and Shanklin, J. D.: Large losses of total ozone in Antarctica reveal seasonal ClO_x/NO_x interaction, Nature, 315, 207–210, 1985.

Hanson, D. and Mauersberger, K.: Laboratory studies of the nitric acid trihydrate: implications for the south polar stratosphere, Geophys. Res. Lett., 15, 855–858, 1988.

Hanson, D. R. and Ravishankara, A. R.: Reactive uptake of $ClONO_2$ onto sulfuric acid due to reaction with HCl and H_2O, J. Phys. Chem., 98, 5728–5735, 1994.

Hoyle, C. R., Engel, I., Luo, B. P., Pitts, M. C., Poole, L. R., Grooß, J.-U., and Peter, T.: Heterogeneous formation of polar stratospheric clouds – Part 1: Nucleation of nitric acid trihydrate (NAT), Atmos. Chem. Phys., 13, 9577–9595, doi:10.5194/acp-13-9577-2013, 2013.

Iraci, L. T., Middlebrook, A. M., and Tolbert, M. A.: Laboratory studies of the formation of polar stratospheric clouds: nitric acid condensation on thin sulphuric acid films, J. Geophys. Res., 100, 20969–20977, 1995.

Koop, T., Biermann, U. M., Raber, W., Luo, B. P., Crutzen, P. J., and Peter, T.: Do stratospheric aerosol droplets freeze above the ice frost point?, Geophys. Res. Lett., 22, 917–920, 1995.

Koop, T., Carslaw, K. S., and Peter, T.: Thermodynamic stability and phase transitions of PSC particles, Geophys. Res. Lett., 24, 2199–2202, 1997.

ACPD
15, 22141–22182, 2015

Lambert, A., Santee, M. L., Wu, D. L., and Chae, J. H.: A-train CALIOP and MLS observations of early winter Antarctic polar stratospheric clouds and nitric acid in 2008, Atmos. Chem. Phys., 12, 2899–2931, doi:10.5194/acp-12-2899-2012, 2012.

Larsen, N., Knudsen, B. M., Rosen, J. M., Kjome, N. T., Neuber, R., and Kyrö, E.: Temperature histories in liquid and solid polar stratospheric cloud formation, J. Geophys. Res., 102, 23505–23517, 1997.

Larsen, N., Knudsen, B. M., Svendsen, S. H., Deshler, T., Rosen, J. M., Kivi, R., Weisser, C., Schreiner, J., Mauerberger, K., Cairo, F., Ovarlez, J., Oelhaf, H., and Spang, R.: Formation of solid particles in synoptic-scale Arctic PSCs in early winter 2002/2003, Atmos. Chem. Phys., 4, 2001–2013, doi:10.5194/acp-4-2001-2004, 2004.

Lehmann, R., von der Gathen, P., Rex, M., and Streibel, M.: Statistical analysis of the precision of the Match method, Atmos. Chem. Phys., 5, 2713–2727, doi:10.5194/acp-5-2713-2005, 2005.

Livesey, N., Van Snyder, W., Read, W., and Wagner, P.: Retrieval algorithms for the EOS Microwave Limb Sounder (MLS), IEEE T. Geosci. Remote, 44, 1144–1155, doi:10.1109/TGRS.2006.872327, 2006.

Livesey, N. J., Read, W. G., Froidevaux, L., Lambert, A., Manney, G. L., Pumphrey, H. C., Santee, M. L., Schwartz, M. J., Wang, S., Cofeld, R. E., Cuddy, D. T., Fuller, R. A., Jarnot, R. F., Jiang, J. H., Knosp, B. W., Stek, P. C., Wagner, P. A., and Wu, D. L.: Version 3.3 and 3.4 Level 2 data quality and description document, D-33509, Jet Propulsion Laboratory, available at: http://mls.jpl.nasa.gov/ (last access: 5 August 2015), 2013.

Marti, J. and Mauersberger, K.: A survey and new measurements of ice vapour pressure at temperatures between 170 and 250 K, Geophys. Res. Lett., 20, 363–366, 1993.

Molina, L. T. and Molina, M. J.: Production of Cl_2O_2 from the self-reaction of the ClO radical, J. Phys. Chem., 91, 433–436, 1987.

Müller, R., Peter, Th., Crutzen, P. J., Oelhaf, H., Adrian, G. P., v. Clarmann, Th., Wegner, A., Schmidt, U., and Lary, D.: Chlorine chemistry and the potential for ozone depletion in the arctic stratosphere in the winter of 1991/92, Geophys. Res. Lett., 21, 1427–1430, 1994.

Pagan, K. L., Tabazadeh, A., Drdla, K., Hervig, M. E., Eckermann, S. D., Browell, E. V., Legg, M. J., and Foschi, P. G.: Observational evidence against mountain-wave generation of ice nuclei as a prerequisite for the formation of three solid nitric acid polar stratospheric clouds observed in the Arctic in early December 1999, J. Geophys. Res., 109, D04312, doi:10.1029/2003JD003846, 2004.

ACPD
15, 22141–22182, 2015

Peter, T. and Grooß, J.-U.: Polar stratospheric clouds and sulfate aerosol particles: microphysics, denitrification and heterogeneous chemistry, in: Stratospheric Ozone Depletion and Climate Change, edited by; Müller, R., Royal Society of Chemistry, 2012.

Pitts, M. C., Thomason, L. W., Poole, L. R., and Winker, D. M.: Characterization of Polar Stratospheric Clouds with spaceborne lidar: CALIPSO and the 2006 Antarctic season, Atmos. Chem. Phys., 7, 5207–5228, doi:10.5194/acp-7-5207-2007, 2007.

Pitts, M. C., Poole, L. R., and Thomason, L. W.: CALIPSO polar stratospheric cloud observations: second-generation detection algorithm and composition discrimination, Atmos. Chem. Phys., 9, 7577–7589, doi:10.5194/acp-9-7577-2009, 2009.

Pitts, M. C., Poole, L. R., Dörnbrack, A., and Thomason, L. W.: The 2009–2010 Arctic polar stratospheric cloud season: a CALIPSO perspective, Atmos. Chem. Phys., 11, 2161–2177, doi:10.5194/acp-11-2161-2011, 2011.

Sander, S. P., Abbatt, J., Barker, J. R., Burkholder, J. B., Friedl, R. R., Golden, D. M., Huie, R. E., Kolb, C. E., Kurylo, M. J., Moortgat, G. K., Orkin, V. L., and Wine, P. H.: Chemical kinetics and photochemical data for use in atmospheric studies, Evaluation Number 17, JPL Publication 10-06, Jet Propulsion Laboratory, California Institute of Technology, Pasadena, available at: http://jpldataeval.jpl.nasa.gov (last access: 5 August 2015), 2011.

Solomon, S., Garcia, R. R., Rowland, F. S., and Wuebbles, D. J.: On the depletion of Antarctic ozone, Nature, 321, 755–758, 1986.

Voigt, C., Schreiner, J., Kohlmann, A., Zink, P., Mauersberger, K., Larsen, N., Deshler, T., Kröger, C., Rosen, J., Adriani, A., Cairo, F., Di Donfrancesco, G., Viterbini, M., Ovarlez, J., Ovarlez, H., David, C., and Dörnbrack, A.: Nitric acid trihydrate (NAT) in polar stratospheric clouds, Science, 290, 1756–1758, 2000.

Voigt, C., Schlager, H., Luo, B. P., Dörnbrack, A., Roiger, A., Stock, P., Curtius, J., Vössing, H., Borrmann, S., Davies, S., Konopka, P., Schiller, C., Shur, G., and Peter, T.: Nitric Acid Trihydrate (NAT) formation at low NAT supersaturation in Polar Stratospheric Clouds (PSCs), Atmos. Chem. Phys., 5, 1371–1380, doi:10.5194/acp-5-1371-2005, 2005.

Waters, J. W., Froidevaux, L., Harwood, R. S., Jarnot, R. F., Pickett, H. M., Read, W. G., Siegel, P. H., Coeld, R. E., Filipiak, M. J., Flower, D. A., Holden, J. R., Lau, G. K., Livesey, N. J., Manney, G. L., Pumphrey, H. C., Santee, M. L., Wu, D. L., Cuddy, D. T., Lay, R. R., Loo, M. S., Perun, V. S., Schwartz, M. J., Stek, P. C., Thurstans, R. P., Chandra, K. M., Chavez, M. C., Chen, G.-S., Boyles, M. A., Chudasama, B. V., Dodge, R., Fuller, R. A., Girard, M. A., Jiang, J. H., Jiang, Y., Knosp, B. W., LaBelle, R. C., Lam, J. C.,

ACPD
15, 22141–22182, 2015

Lee, K. A., Miller, D., Oswald, J. E., Patel, N. C., Pukala, D. M., Quintero, O., Scaff, D. M., Snyder, W. V., Tope, M. C., Wagner, P. A., and Walch, M. J.: The Earth Observing System Microwave Limb Sounder (EOS MLS) on the Aura satellite, IEEE T. Geosci. Remote, 44, 1075–1092, 2006.

Wegner, T., Grooß, J.-U., von Hobe, M., Stroh, F., Sumińska-Ebersoldt, O., Volk, C. M., Hösen, E., Mitev, V., Shur, G., and Müller, R.: Heterogeneous chlorine activation on stratospheric aerosols and clouds in the Arctic polar vortex, Atmos. Chem. Phys., 12, 11095–11106, doi:10.5194/acp-12-11095-2012, 2012.

Winker, D. M., McGill, M., and Hunt, W. H.: Initial performance assessment of CALIOP, Geophys. Res. Lett., 34, L19803, doi:10.1029/2007GL030135, 2007.

Winker, D. M., Vaughan, M. A., Omar, A. H., Hu, Y., Powell, K. A., Liu, Z., Hunt, W. H., and Young, S. A.: Oberview of the CALIPSO mission and CALIOP data processing algorithms, J. Atmos. Ocean. Tech., 26, 2310–2323, doi:10.1175/2009JTECHA1281.1, 2009.

Wohltmann, I., Lehmann, R., and Rex, M.: The Lagrangian chemistry and transport model ATLAS: simulation and validation of stratospheric chemistry and ozone loss in the winter 1999/2000, Geosci. Model Dev., 3, 585–601, doi:10.5194/gmd-3-585-2010, 2010.

Wohltmann, I., Wegner, T., Müller, R., Lehmann, R., Rex, M., Manney, G. L., Santee, M. L., Bernath, P., Sumińska-Ebersoldt, O., Stroh, F., von Hobe, M., Volk, C. M., Hösen, E., Ravegnani, F., Ulanovsky, A., and Yushkov, V.: Uncertainties in modelling heterogeneous chemistry and Arctic ozone depletion in the winter 2009/2010, Atmos. Chem. Phys., 13, 3909–3929, doi:10.5194/acp-13-3909-2013, 2013.

ACPD
15, 22141–22182, 2015

Table 1. List of the selected cases for the trajectory runs. The first column shows the ID number of the case used in the following analysis, the second column shows the starting date, and the third column the starting time of the trajectory. The remaining columns show the location of the starting position (t = 0) of the forward and backward trajectories.

Case ID	Date	Time (UT)	latitude (N)	longitude (E)	altitude (km)	PT (K)	Pressure (hPa)
#01	19 December 2009	16:37:56	79.85	263.71	22.36	520.9	31.60
#02	21 December 2009	08:09:30	75.50	50.54	22.97	559.2	27.91
#03	23 December 2009	07:58:21	78.90	39.92	22.07	526.0	31.60
#04	23 December 2009	07:58:45	79.85	33.50	22.05	522.9	31.60
#05	30 December 2009	17:53:38	66.13	279.29	22.97	546.4	27.44
#06	31 December 2009	08:58:26	57.56	264.93	21.00	511.8	40.68
#07	31 December 2009	12:10:25	76.70	241.31	22.15	531.7	31.60
#08	31 December 2009	16:59:14	70.28	288.19	24.05	565.3	22.61
#09	31 December 2009	18:35:15	60.44	273.13	24.95	612.4	19.84
#10	1 January 2010	09:39:12	66.12	260.59	22.97	551.0	27.60
#11	1 January 2010	17:41:15	66.12	282.38	24.05	570.7	23.24

ACPD
15, 22141–22182, 2015

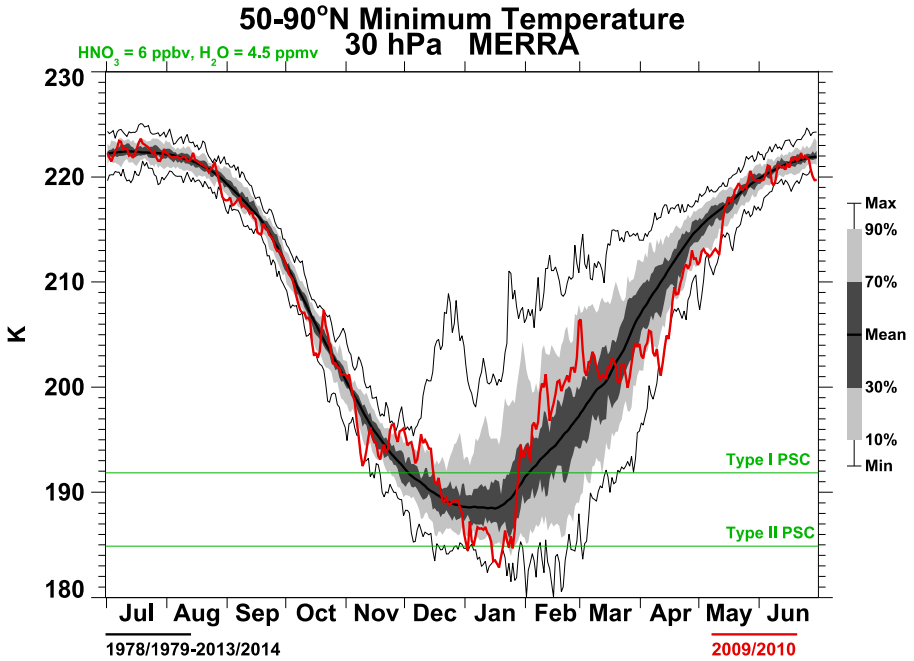

Figure 1. Variation of the minimum temperature (50–90° N) in the Arctic stratosphere at 30 hPa by Modern Era Retrospective-Analysis (MERRA) data. The thick black line shows the average minimum temperature between 1978/79 and 2013/14, while the thick and thin shaded area represents 30–70 and 10–90 % percentile distributions, respectively. The red line shows the minimum temperature in the 2009/10 Arctic winter. Two horizontal green lines represent the Type I (NAT) PSC threshold temperature assuming 6 ppbv HNO_3 and 4.5 ppmv H_2O, and the ice frost point temperature, respectively.

ACPD
15, 22141–22182, 2015

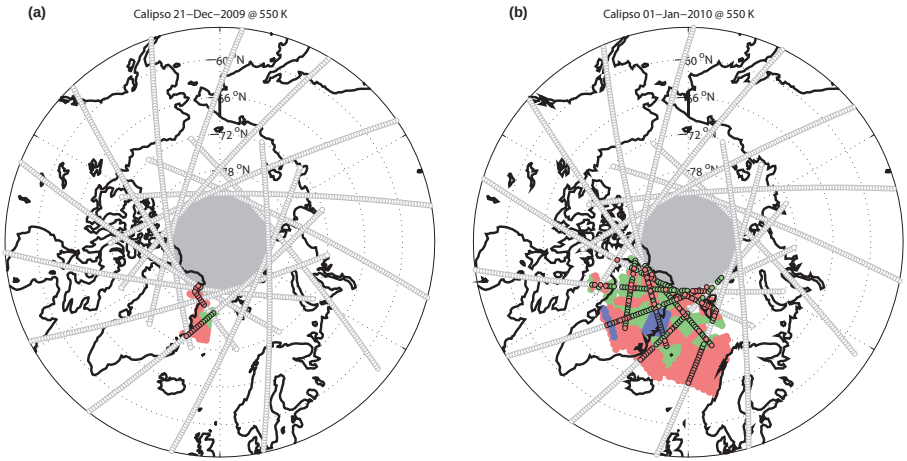

Figure 2. CALIOP PSC field for 21 December 2009 **(a)** and for 1 January 2010 **(b)** at the 550 K potential temperature surface. The green area represents STS PSCs, the red area mixed NAT and STS PSCs, and the blue area ice PSCs. Grey and black circles show CALIOP observation points for nighttime orbit segments. No measurements are available in the grey area around the pole (> 82° N) due to the orbital coverage of the CALIPSO satellite.

ACPD
15, 22141–22182, 2015

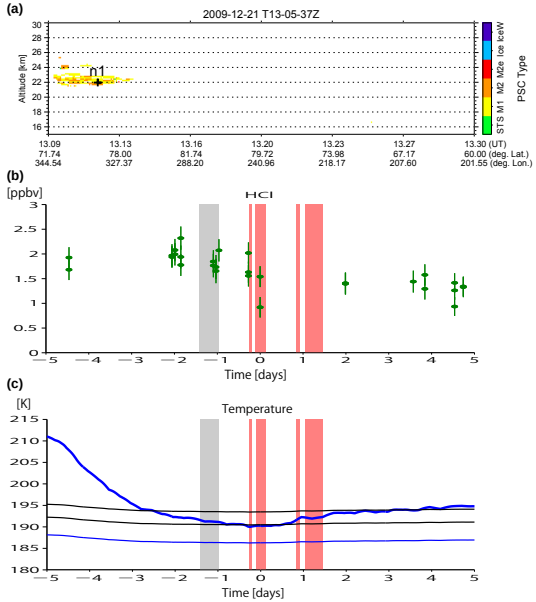

Figure 3. (a) Time-altitude plot of the PSC distribution on 21 December 2009 from 13.09 to 13.30 UTC (fractional hours). PSC classifications are color coded (STS, M1: Mix 1, M2: Mix 2, M2e: Mix 2 enhanced, Ice, IceW: Wave Ice, for details see Pitts et al., 2011). The labels on the horizontal axis show fractional time, latitude and longitude. The cross with "n1" denotes the starting point of the forward/backward trajectories of panels **(b)** and **(c)** where mix 1 PSC was present. **(b)** HCl measurements by MLS (green dots with error bars) along 5 day forward and 5 day backward trajectories starting at the cross in panel **(a)**. The match radius between MLS measurements and the trajectory is 200 km. The color coded areas show PSC occurrence measured by CALIOP along the trajectories, with the same color code as in Fig. 2. Time is given relative to the trajectory starting time. **(c)** Temperature along the trajectories (blue line). The thin black lines show the threshold temperature for NAT formation T_{NAT} and $T_{NAT} - 3$ K. The thin blue line shows T_{ice}.

ACPD
15, 22141–22182, 2015

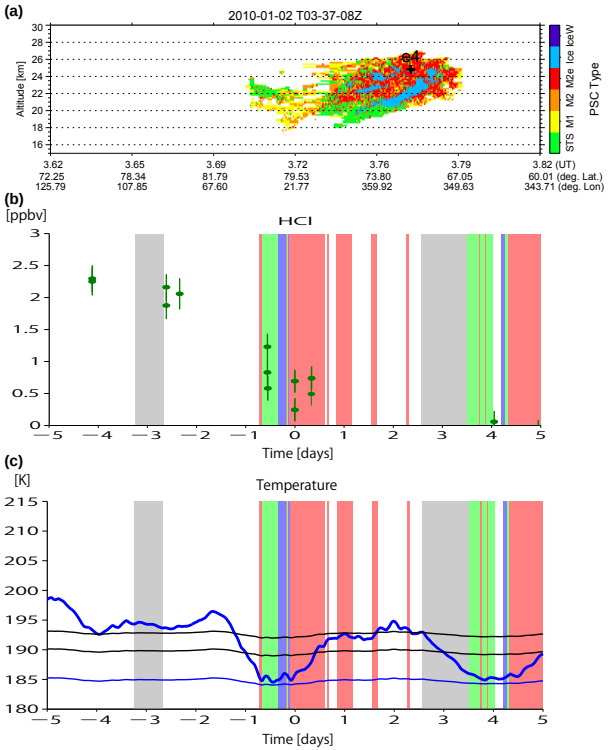

Figure 4. Same as Fig. 3 but for 2 January 2010 from 3.63 to 3.82 UTC. The cross with "e4" denotes the starting point of forward/backward trajectories where mix 2 enhanced PSC was present.

ACPD
15, 22141–22182, 2015

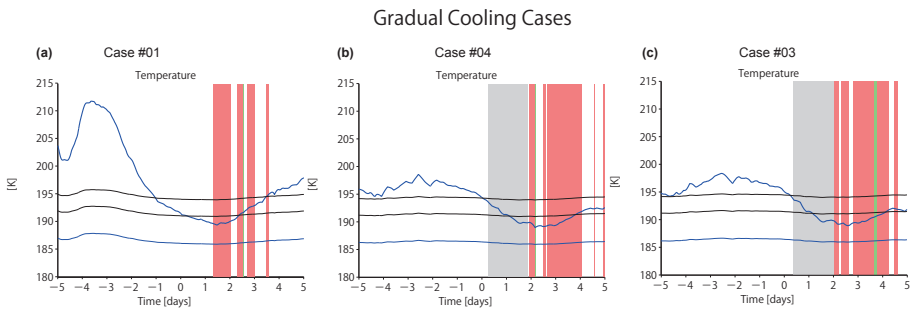

Figure 5. Temperature along the trajectories for the cases #01 **(a)**, #04 **(b)** and #03 **(c)** listed in Table 1. The color coded areas show PSC occurrence measured by CALIOP along the trajectories, with the same color code as in Fig. 2. Shaded grey area represents that PSC types were unknown due to the CALIPSO orbital limitation (> 82° N). The thin black lines show the threshold temperature for NAT formation T_{NAT} and $T_{NAT} - 3$ K. The thin blue line shows T_{ice}.

ACPD
15, 22141–22182, 2015

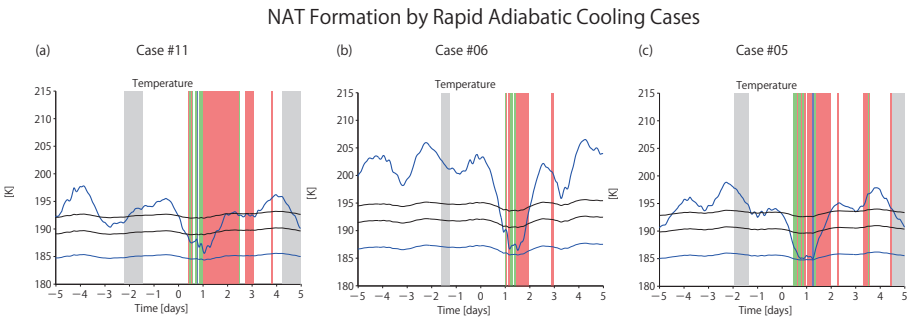

Figure 6. Same as Fig. 5 but for trajectory cases #11 **(a)**, #06 **(b)**, and #05 **(c)**, respectively.

ACPD
15, 22141–22182, 2015

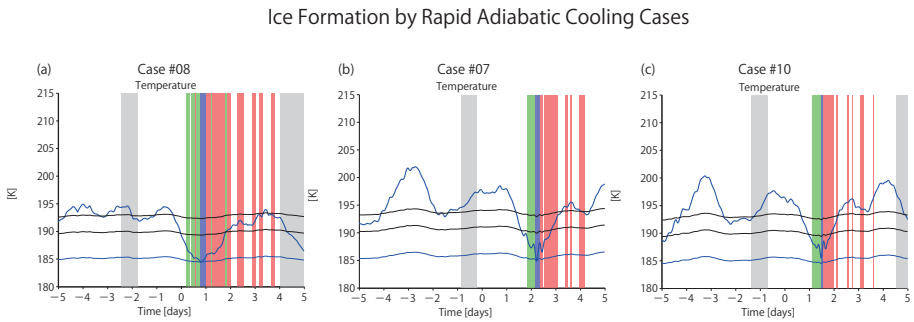

Figure 7. Same as Fig. 5 but for trajectory cases #08 **(a)**, #07 **(b)**, and #10 **(c)**, respectively.

ACPD
15, 22141–22182, 2015

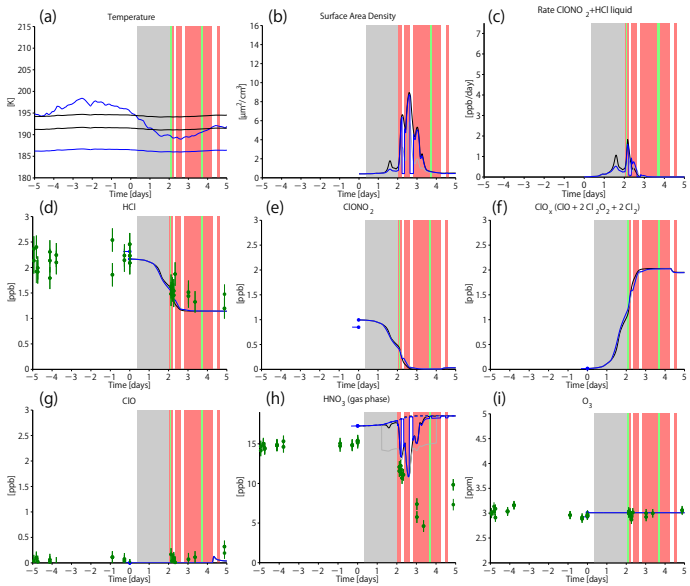

Figure 8. Results of the ATLAS chemistry model along the trajectories and comparison with measurements by MLS for the trajectory case #03 starting on 23 December 2009 at 07:58:21 UT. **(a)** Temperature (as in Figs. 5–7), **(b)** PSC surface area density, **(c)** $ClONO_2$ + HCl heterogeneous reaction rate, **(d)** HCl mixing ratio, **(e)** $ClONO_2$ mixing ratio, **(f)** ClO_x (ClO + 2 × Cl_2O_2 + 2× Cl_2) mixing ratio, **(g)** ClO mixing ratio, **(h)** HNO_3 mixing ratio, and **(i)** O_3 mixing ratio. Matched MLS measurements of HCl, ClO, HNO_3 and O_3 are shown in panels **(d)**, **(g)**, **(h)** and **(i)** (green dots with error bars). Panel **(b)** to **(i)** show model results of the ATLAS chemistry model for the "STS + NAT" run (black curve), the "STS" run (grey curve) and the "CALIPSO constrained" run (blue curve). The color coded areas show PSC occurrence measured by CALIOP along the trajectories, with the same color code as in Fig. 2.

ACPD
15, 22141–22182, 2015

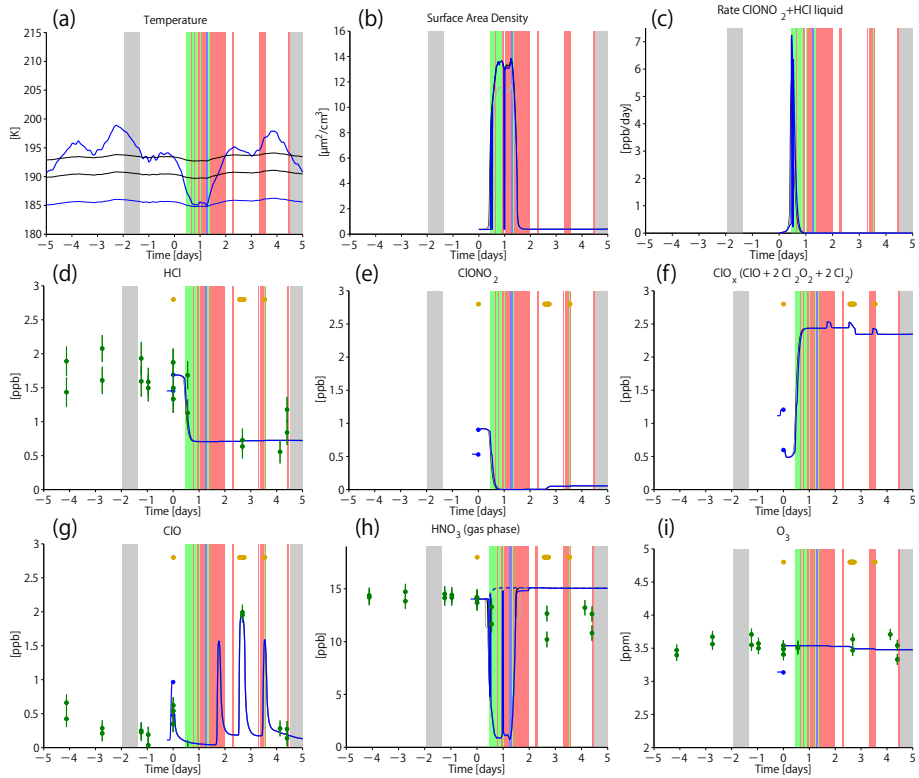

Figure 9. Same as Fig. 8 but for trajectory case #05 starting on 30 December 2009 at 17:53:38 UT. The orange dots in panels **(d–i)** indicate the period of solar illumination when the solar zenith angle is smaller than 90°.

ACPD
15, 22141–22182, 2015

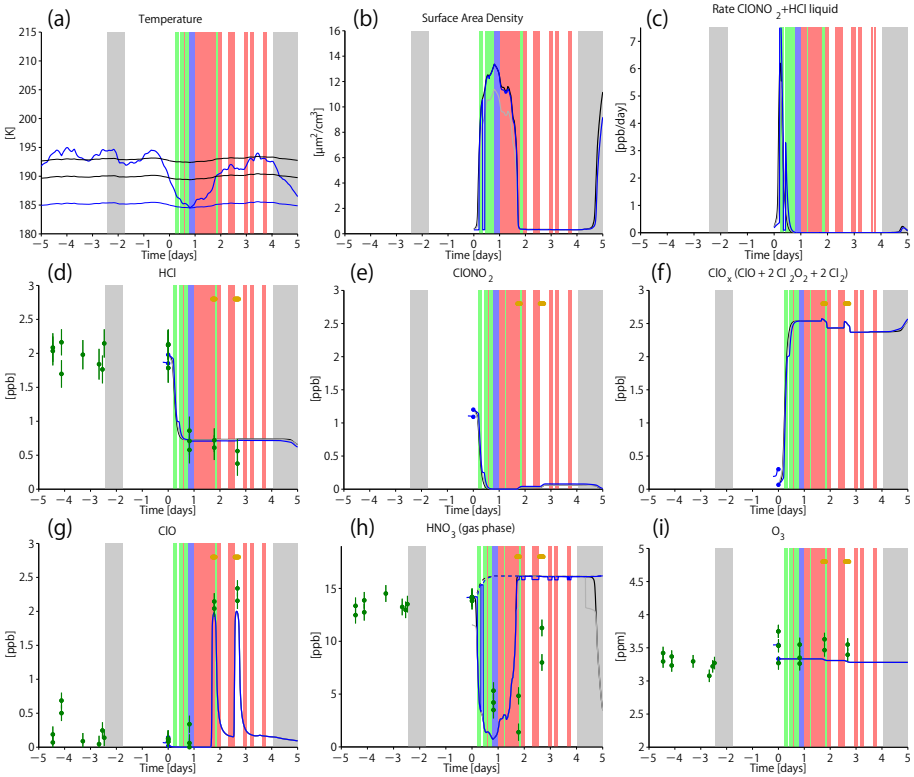

Figure 10. Same as Fig. 8 but for trajectory case #08 starting on 31 December 2009 at 16:59:14 UT.

ACPD
15, 22141–22182, 2015

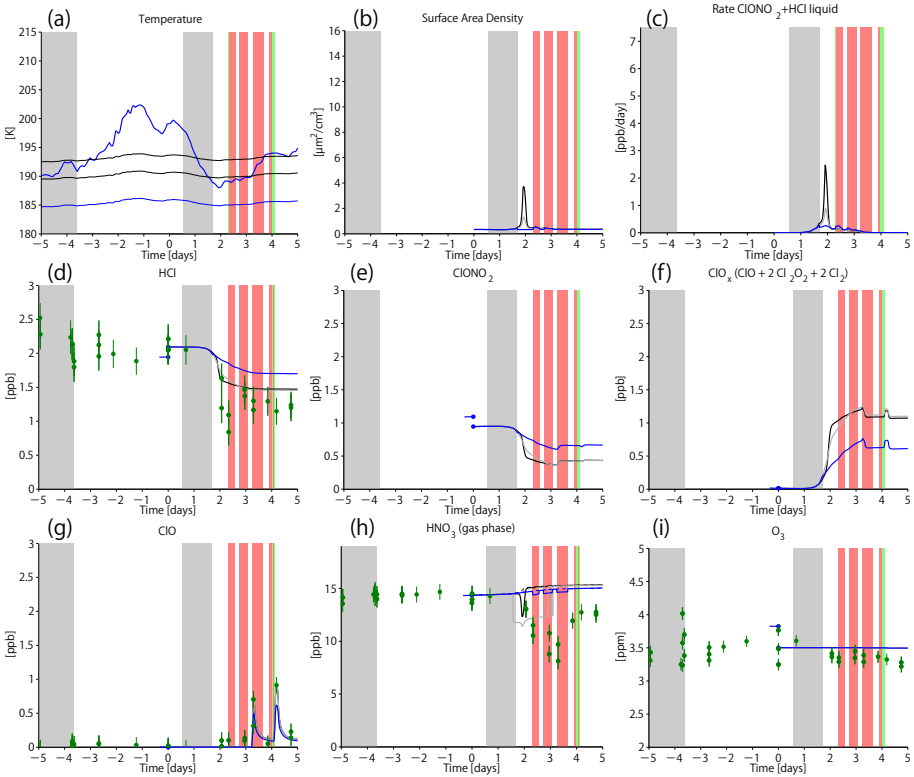

Figure 11. Same as Fig. 8 but for trajectory case #02 starting on 21 December 2009 at 08:09:30 UT.

ACPD
15, 22141–22182, 2015

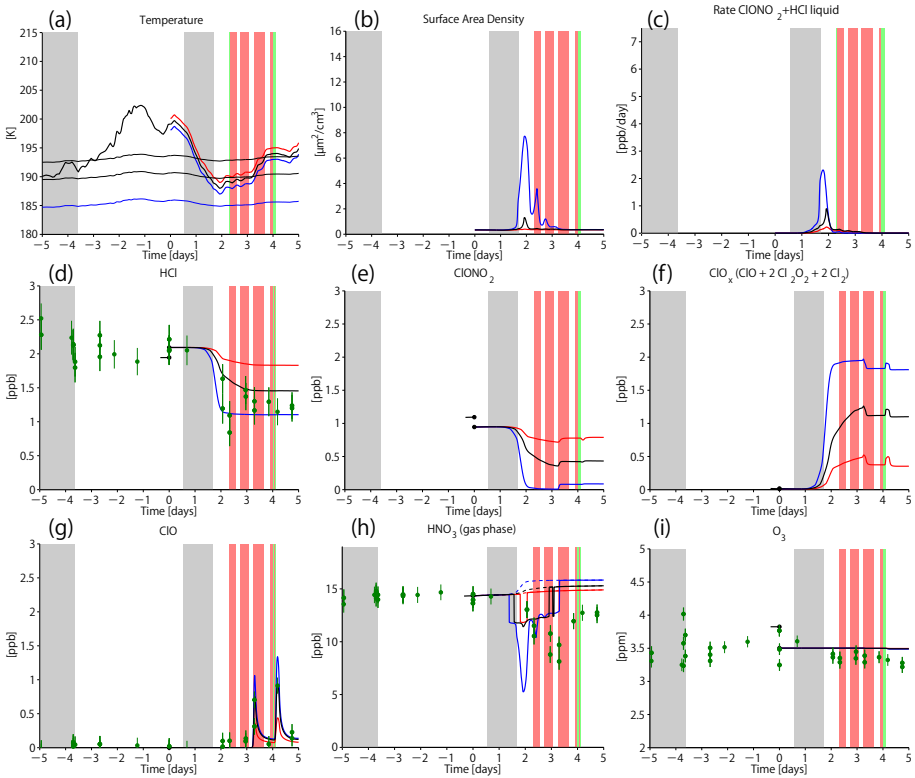

Figure 12. Temperature sensitivity runs for trajectory case #02. The black line shows the "STS + NAT" run, the red line a sensitivity run with temperature increased by 1 K and the blue line a sensitivity run with temperature decreased by 1 K. MLS measurements and PSC types are the same as in Fig. 11.

ACPD
15, 22141–22182, 2015

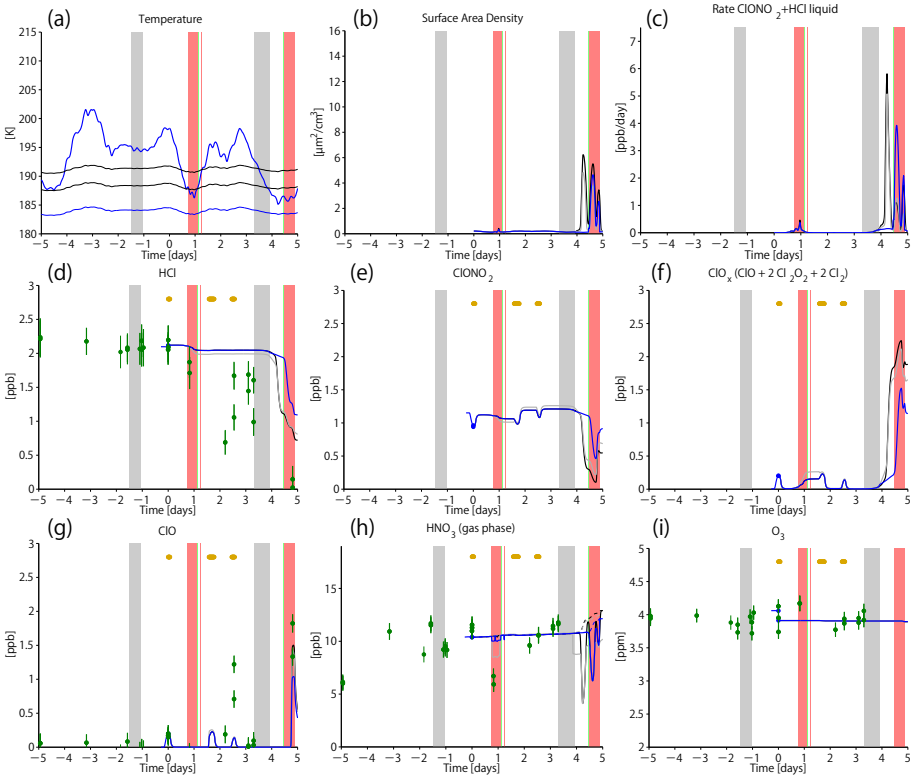

Figure 13. Same as Fig. 8 but for trajectory case #09 starting on 31 December 2009 at 18:35:15 UT.

ACPD
15, 22141–22182, 2015

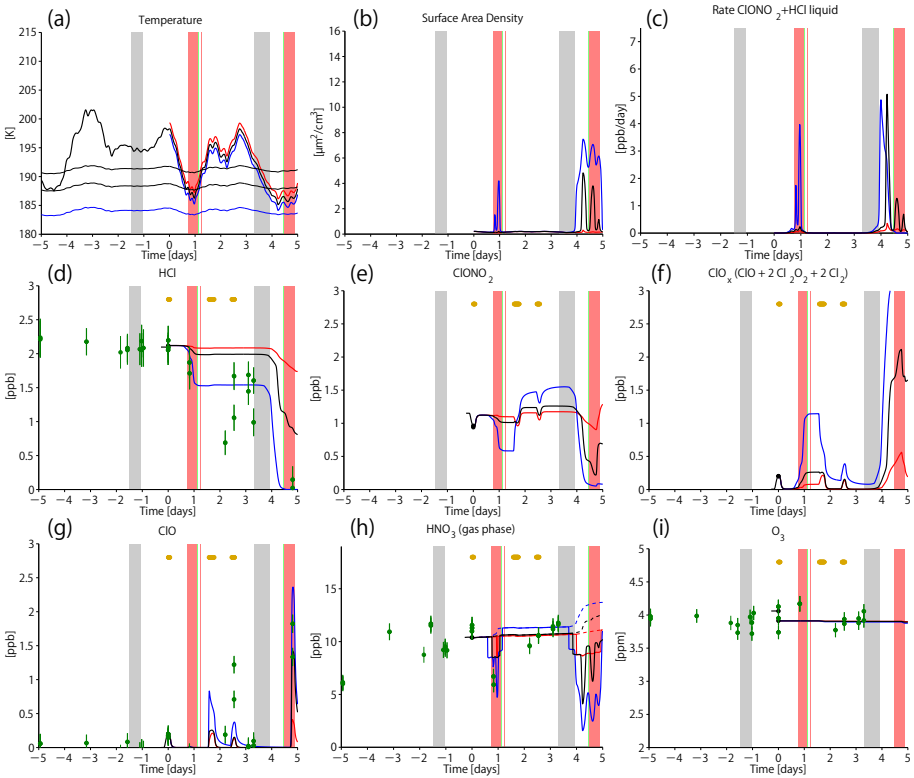

Figure 14. Temperature sensitivity runs for trajectory case #09. Line colors here are the same as those in Fig. 12.

ACPD
15, 22141–22182, 2015

PSC evolution and Cly activation by CALIPSO, MLS and ATLAS

H. Nakajima et al.